LETTERS

Non-volcanic tremor driven by large transient shear stresses

Justin L. Rubinstein[1], John E. Vidale[1], Joan Gomberg[2], Paul Bodin[1], Kenneth C. Creager[1] & Stephen D. Malone[1]

Non-impulsive seismic radiation or 'tremor' has long been observed at volcanoes[1] and more recently around subduction zones[2]. Although the number of observations of non-volcanic tremor is steadily increasing, the causative mechanism remains unclear. Some have attributed non-volcanic tremor to the movement of fluids[2–6], while its coincidence with geodetically observed slow-slip events at regular intervals[7,8] has led others to consider slip on the plate interface as its cause[7–14]. Low-frequency earthquakes in Japan, which are believed to make up at least part of non-volcanic tremor[9], have focal mechanisms[10] and locations[11] that are consistent with tremor being generated by shear slip on the subduction interface. In Cascadia, however, tremor locations appear to be more distributed in depth than in Japan[3,4], making them harder to reconcile with a plate interface shear-slip model. Here we identify bursts of tremor that radiated from the Cascadia subduction zone near Vancouver Island, Canada, during the strongest shaking from the moment magnitude $M_w = 7.8$, 2002 Denali, Alaska, earthquake. Tremor occurs when the Love wave displacements are to the southwest (the direction of plate convergence of the overriding plate), implying that the Love waves trigger the tremor. We show that these displacements correspond to shear stresses of approximately 40 kPa on the plate interface, which suggests that the effective stress on the plate interface is very low. These observations indicate that tremor and possibly slow slip can be instantaneously induced by shear stress increases on the subduction interface—effectively a frictional failure response to the driving stress.

To understand the source physics of non-volcanic tremor we need to know how it initiates, and more specifically whether it can be initiated by dynamic stresses. Obara[2] identified three different earthquakes of local magnitude $M_J \geq 5$ that may have triggered tremor. Following this initial study, Obara[15] identified many more earthquakes that may have triggered tremor, including local microearthquakes ($2 \leq M_J \leq 3$), local medium magnitude earthquakes ($3 \leq M_J \leq 6.5$), and large earthquakes ($M_w \geq 7.0$ at $>1{,}000$ km).

These findings led Miyazawa and Mori to closely examine tremor triggered by the $M_w = 8.3$ Tokachi-Oki[16] and the 2004 Sumatra earthquakes[17]. For the specific geometry of the Sumatra earthquake and its orientation relative to the Japanese subduction zone, dilatational stresses associated with the Rayleigh wave were inferred to be much more effective than horizontal shear stresses in triggering tremor[17]. On the basis of this finding, it was hypothesized that fluid flow facilitates tremor[17,18].

Inspired by the above findings, we examined seismic recordings of the 3 November 2002 $M_w = 7.8$ Denali earthquake, which triggered seismicity throughout much of western North America[19]. In this case, directivity focused and amplified seismic waves towards western North America, especially the Love waves[19,20]. Examining these seismograms, we found clear evidence of triggered tremor near Vancouver Island.

The tectonics of the region are dominated by the slow subduction of the Juan de Fuca and Explorer plates underneath the North American plate, with the trench located off the west coast of Vancouver Island[21] (Fig. 1). This subduction zone is well known because it is the place where episodic tremor and slip (ETS), the repeated coincidence of geodetically observed slow-slip and elevated levels of non-volcanic tremor at regular intervals, was first discovered[7]. Non-volcanic tremor has been observed running almost the entire length of Vancouver Island[3,22]. Examining the seismic records of the Denali earthquake in Vancouver Island, we identified shaking-induced tremor bursts in northern Vancouver Island. There are indications that tremor was also triggered on Southern Vancouver Island, but it was overprinted by stronger, triggered earthquake activity. Thus, we focused on the northern region.

In the recordings of the Denali mainshock at high frequencies we can identify Denali's *P* waves, locally triggered tremor and locally triggered earthquakes (Fig. 2). At low frequencies the Love and Rayleigh waves from Denali are visible. The tremor appeared in five bursts that peaked at 310, 345, 365, 386 and 415 s at station PHC, with distinct gaps between some of the bursts. There are additional patterns of high-frequency energy that differed for each station, especially in the interval from 425 to 500 s, whose origin is not clear. The

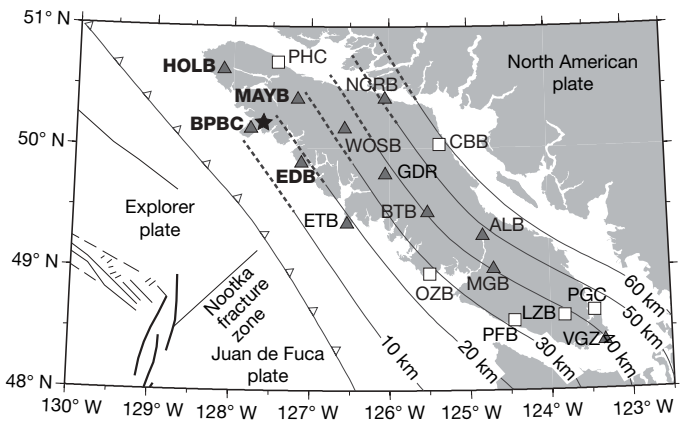

Figure 1 | Map of Vancouver Island. Local geologic features, Canadian National Seismic Network (CNSN) stations on the island (white squares, broadband; grey triangles, short period), and the location of the triggered tremor (black star) are indicated on the map. The stations we used to locate the triggered tremor are indicated with bold type. Solid lines indicate isodepths (shown in kilometres) of the interface between the Juan de Fuca and the North American plates; dotted lines indicate isodepths of the interface between the Explorer and the North American plates; solid line with triangles indicates the location of the plate interface at the earth's surface. Figure modified with permission from figure 1b in ref. 22.

[1]Department of Earth and Space Science, [2]United States Geological Survey, University of Washington, Box 351310, Seattle, Washington, 98195, USA.

five bursts were similar across many stations and had a move-out consistent with a single location (Supplementary Fig. 1). The relative timing of the tremor arrivals differed from that of the through-going Denali surface waves, so we can be sure that the tremor is not an artefact of filtering or an instrumental effect caused by large amplitudes. The simultaneous arrival of the Rayleigh waves and the tremor at station PHC is merely a coincidence, because their relative timing has not yet been corrected for different source locations and propagation velocities.

Our triggered tremor observations cover the broad range of frequencies 4–30 Hz with signal-to-noise ratio exceeding 10:1. In contrast, observations of tremor during an ETS episode ('ETS tremor') are strongest in a narrower band (1–10 Hz). We examined other reported incidences of earthquake-triggered tremor[16,17] and found similarly high signal amplitudes for a broad range of frequencies. While the visible bandwidth of triggered and ETS tremor is different, spectral comparison revealed that both have a similar high-frequency spectral shape (Supplementary Fig. 2), with the larger signal-to-noise ratio of the triggered tremor making it visible at a broader range of frequencies. It follows that ETS tremor and triggered tremor may be generated by the same physical process. We note that while the spectra of the triggered tremor diverges from the ETS tremor below 2 Hz, this difference arises because the triggered tremor is superposed on lower-frequency *S* coda and surface waves from the Denali earthquake. Like previous studies[2,3,9], we found that tremor is deficient in high frequencies relative to earthquakes.

We located the tremor by a search over a grid of possible locations, cross-correlating the envelopes from the four best recordings of a window containing the three largest bursts of tremor. This method is similar to that used by Obara[2]. We corrected the known-to-be-erroneous timing at stations HOLB and EDB by 13 s and 102 s respectively. These figures were determined from phase-arrival residuals of local earthquakes occurring on the same day as the Denali earthquake. The epicentral location of the tremor is tightly constrained to be 50.19°N ± 6 km and 127.61°W ± 4 km (Fig. 1). The source depth is loosely constrained to lie between 10 and 34 km. Epicentral locations obtained for the first and second bursts place them approximately 10 and 6 km to the southwest of the joint location for bursts 2 to 4. This suggests that the tremor may have migrated in a northeasterly direction. The triggered tremor is located further north and more up-dip than the majority of ETS tremor in the region[22]. This may indicate that slightly different conditions are needed to produce triggered tremor rather than ETS tremor.

To understand the triggering relationship between the surface waves and the tremor, we take the location of the tremor and shift the tremor and surface waves seismograms such that they directly reflect the timing relationship at the source location of the tremor (Fig. 3). The first four bursts of tremor were clearly triggered by the Love waves, but the Rayleigh waves arrived in time possibly to contribute to the fourth and fifth bursts. The tremor occurred when the Love wave displacement was southwest, but halted when the displacement reversed to the northeast. This is the expected polarity if the ambient stress field causes tremor, that is, when the Love waves from Denali amplified the shear stress in the direction of plate motion on the subduction interface. The amplitude of the triggered tremor also appears to scale with the up-dip shear stress of the Love waves resolved onto the plate interface.

The geometry of the Denali earthquake and Cascadia subduction zone is unique in that the surface waves from Denali propagated parallel to the strike of the subduction zone. This means that the Love waves are polarized such that their motions are parallel to the convergence direction and the Rayleigh wave motions oscillate parallel to the subduction zone strike. This geometry directs nearly all of the shear stress associated with the Love wave to alternately promoting and resisting plate convergence, while less of the stress associated with the Rayleigh wave directly affects plate convergence. This unique geometry and the fact that the Love waves are much larger than the Rayleigh waves explains why the Love waves triggered tremor and the Rayleigh waves did not.

We quantified the stresses and their timing on the subduction interface using synthetic seismograms that match the surface waves of the Denali earthquake on Vancouver Island (Supplementary Figs 3 and 4). In this calculation the Love waves caused the maximum shear stress resolved in the updip/downdip direction (43 kPa), while the maximum dilatational stress, which was caused by the Rayleigh waves, was only 12 kPa. The significantly larger shear stresses on the plate interface suggest that they were responsible for the triggering. For dilatation to be responsible for the tremor, it would require the tremor to be at least three times more sensitive to dilatation than shear. Even more compelling evidence for shear-triggered tremor is

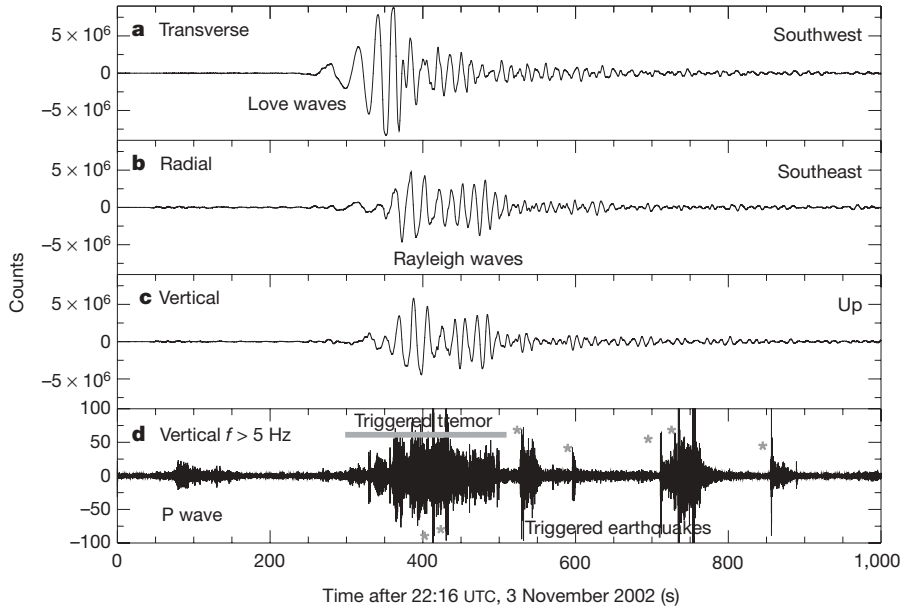

Figure 2 | Broadband, three-component recording of the Denali earthquake and locally triggered tremor and earthquakes. Record from station PHC showing the *P* wave and surface waves from Denali and locally triggered tremor and earthquakes. Raw records for transverse (**a**, 238°) radial (**b**, 148°) and vertical velocity (**c**). **d**, 5 Hz high-pass-filtered vertical velocity trace. Triggered local earthquakes are indicated by grey asterisks in the bottom panel.

that the timing of the tremor pulses and the shear stress increases match, while the Rayleigh waves arrive too late to trigger tremor.

The modest shear stress changes required to trigger tremor suggest several possible conditions within the subduction zone where the tremor occurred: the effective stress (the difference between the normal stress and pore pressure) is very low, the static friction and shear strength are low, and/or the stresses were near critical levels at the time of the Denali earthquake. Evidence from triggered earthquakes leads to similar suggestions. The existence of low effective stresses is consistent with earthquakes in geothermal fields (regions with hot fluids/gas that are presumably under high pressure) triggering under lower dynamic stresses (as low as 5 kPa; ref. 23) than in other crustal regions (of the order of hundreds to thousands of kilopascals; ref. 24). It is also consistent with a theoretical rate-state frictional model of ETS[25]. The recurrence interval of ~14 months between slow slip events in northern Cascadia and estimates showing they relax much (about two-thirds) of the stress accumulated during the interval[26] provide evidence for the second possibility: a weak interface.

We hypothesize that shear stress on the plate interface from the Love waves of the Denali earthquake triggered the tremor. Specifically, by analogy with ETS, we suggest that the shearing caused by the Love waves induced slow shear-failure on the plate interface, radiating the tremor we observe. Thus when the Love waves stressed the fault in the sense of the subduction deformation, the megathrust allowed an increment of subduction-directed fault slip, accompanied by tremor. In other words, tremor reflects a process in which failure follows a simple frictional behaviour. This model is consistent with the observations that the tremor is only triggered when the ambient stress field is amplified and that the tremor amplitude scales with the amplitude of the shear stresses associated with the triggering waves.

Our idea that triggered tremor follows a simple frictional threshold can also be used to explain the observations of triggered tremor that previous authors have attributed to dilatation and fluid flow[17,18]. For those cases where large dilatations are observed coincident with triggered tremor, we argue that the dilatations would also reduce normal stresses on the plate interface, thus increasing the likelihood of frictional failure.

Although we appeal to frictional failure as the physical mechanism responsible for generating the triggered tremor we observe, we still believe fluids to be important: we expect that high fluid pressures within the subduction zone do facilitate the slip. We suggest that the phenomenon we observed—low stress-drop or slow shear-failure in response to dynamically elevated shear stress—may also occur in locations closer to mainshock fault ruptures (where dynamic stresses are large), which implies that it may be important in the rupture process itself.

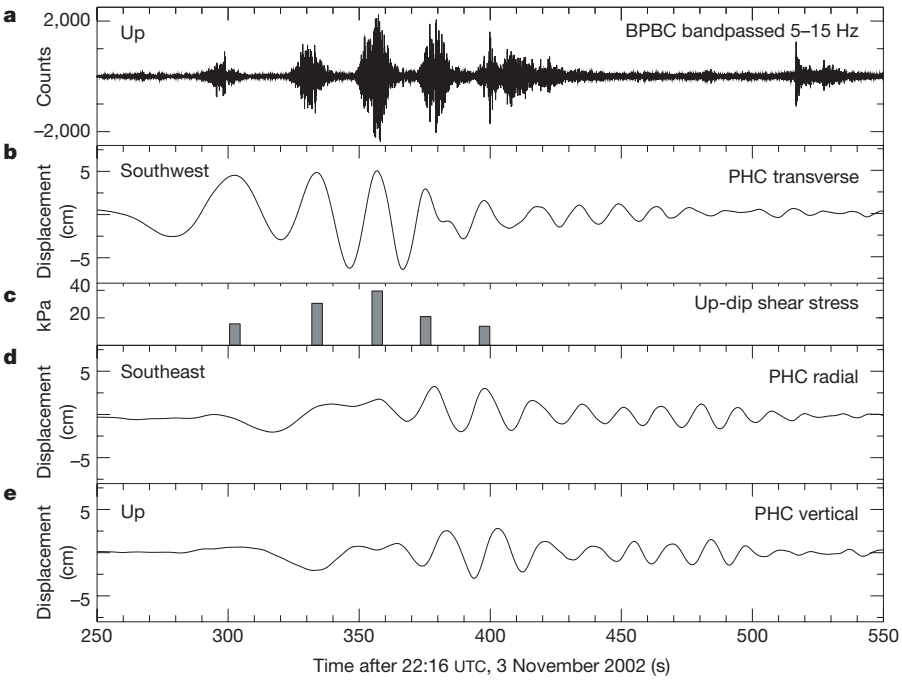

Figure 3 | Comparison of tremor and the surface waves that triggered it at the site where the tremor is radiated. a, Tremor at the closest station BPBC, time-adjusted by 5.14 s to reflect the travel time of *S* waves from the tremor source to BPBC. We used the epicentre determined for the window containing the second to fourth bursts of tremor and a depth of 15 km, the approximate depth of the plate interface, to estimate this travel time. Bursts one and two appear early because a single correction was applied to sources with different locations. Bursts 1 and 2 emanate from a source closer to BPBC than the sources corresponding to the bursts used to derive the correction; their locations would require shifts of ~1.0 and 0.8 s to the right, respectively, aligning them more closely with the triggering surface waves. **b**, **d**, **e**, Instrument-corrected displacement seismograms for the transverse, radial and vertical components at PHC, the closest three-component, broadband station to the tremor, shifted by 8.40 s seconds to reflect the difference in arrival time of the third and largest Love wave pulse at PHC and at the tremor source. The velocity for each triggering Love wave pulse was estimated using its relative arrival times at ten broadband stations on Vancouver Island and on the Canadian mainland. Because surface waves are dispersive—that is, their velocity depends on their wavelength—the correction we have applied is too large for the faster surface wave arrivals (for example, the first triggering pulse should be shifted left ~0.9 s) and too small for the slower surface wave arrivals (for example, the last triggering pulse should be shifted right ~0.5 s). The tremor appears to turn on when displacement is to the southwest and turn off when it is to the northeast, suggesting that the strains induced by the passage of the Love waves modulated the tremor. **c**, Predicted maximum shear stress on the plate interface from the five triggering Love wave pulses is plotted as a vertical bar centred on the maximum of each pulse. The shear stress values do not have a 1:1 relationship with the observed displacements because the stresses induced by a surface wave depend on the period of the waves. In this geometry, as the period of the Love waves increases, the shear stress on the plate interface decreases (Supplementary Fig. 5). Using a transfer function from surface displacement to shear stress on the plate interface determined from the synthetic seismograms (Supplementary Figs 3 to 5), we estimate the amount of shear stress on the plate interface by determining the period and maximum amplitude of the five triggering bursts from the displacement seismograms at PHC.

Received 28 February; accepted 13 June 2007.

1. McNutt, S. R. Volcanic seismology. *Annu. Rev. Earth Planet. Sci.* **33,** 461–491 (2005).
2. Obara, K. Nonvolcanic deep tremor associated with subduction in southwest Japan. *Science* **296,** 1679–1681 (2002).
3. Kao, H. *et al.* A wide depth distribution of seismic tremors along the northern Cascadia margin. *Nature* **436,** 841–844 (2005).
4. McCausland, W., Malone, S. & Johnson, D. Temporal and spatial occurrence of deep non-volcanic tremor: From Washington to northern California. *Geophys. Res. Lett.* **32,** L24311, doi:10.1029/2005GL024349 (2005).
5. Katsumata, A. & Kamaya, N. Low-frequency continuous tremor around the Moho discontinuity away from volcanoes in the southwest Japan. *Geophys. Res. Lett.* **30,** 1020, doi:10.1029/2002GL015981 (2003).
6. Seno, T. & Yamasaki, T. Low-frequency tremors, intraslab and interplate earthquakes in Southwest Japan—from a viewpoint of slab dehydration. *Geophys. Res. Lett.* **30,** 2171, doi:10.1029/2003GL018349 (2003).
7. Rogers, G. & Dragert, H. Episodic tremor and slip on the Cascadia subduction zone: The chatter of silent slip. *Science* **300,** 1942–1943 (2003).
8. Obara, K., Hirose, H., Yamamizu, F. & Kasahara, K. Episodic slow slip events accompanied by non-volcanic tremors in southwest Japan subduction zone. *Geophys. Res. Lett.* **31,** L26302, doi:10.1029/2004GL020848 (2004).
9. Shelly, D. R., Beroza, G. C. & Ide, S. Non-volcanic tremor and low frequency earthquake swarms. *Nature* **446,** 305–307 (2007).
10. Ide, S., Shelly, D. R. & Beroza, G. C. Mechanism of deep low frequency earthquakes: Further evidence that deep non-volcanic tremor is generated by shear slip on the plate interface. *Geophys. Res. Lett.* **34,** L03308, doi:10.1029/2006GL028890 (2007).
11. Shelly, D. R., Beroza, G. C., Ide, S. & Nakamula, S. Low-frequency earthquakes in Shikoku, Japan, and their relationship to episodic tremor and slip. *Nature* **442,** 188–191 (2006).
12. Ide, S., Beroza, G. C., Shelly, D. R. & Uchide, T. A scaling law for slow earthquakes. *Nature* **447,** 76–79 (2007).
13. Obara, K. & Hirose, H. Non-volcanic deep low-frequency tremors accompanying slow slips in the southwest Japan subduction zone. *Tectonophysics* **417,** 33–51 (2006).
14. Royle, G. T., Calvert, A. J. & Kao, H. Observations of non-volcanic tremor during the northern Cascadia slow-slip event in February 2002. *Geophys. Res. Lett.* **33,** L18313, doi:10.1029/2006GL027316 (2006).
15. Obara, K. Time sequence of deep low-frequency tremors in the Southwest Japan Subduction Zone: Triggering phenomena and periodic activity. [in Japanese] *Chigaku Zasshi (J. Geogr.)* **112,** 837–849 (2003).
16. Miyazawa, M. & Mori, J. Detection of triggered deep low-frequency events from the 2003 Tokachi-oki earthquake. *Geophys. Res. Lett.* **32,** L10307, doi:10.1029/2005GL022539 (2005).
17. Miyazawa, M. & Mori, J. Evidence suggesting fluid flow beneath Japan due to periodic seismic triggering from the 2004 Sumatra-Andaman earthquake. *Geophys. Res. Lett.* **33,** L05303, doi:10.129/2005GL025087 (2006).
18. Miyazawa, M. & Brodsky, E. E. Fluid related deep low-frequency earthquakes resonant with the Rayleigh waves from the 2004 Sumatra-Andaman earthquake. *J. Geophys. Res.* (submitted).
19. Gomberg, J., Bodin, P., Larson, K. & Dragert, H. Earthquake nucleation by transient deformations caused by the $M=7.9$ Denali, Alaska, earthquake. *Nature* **427,** 621–624 (2004).
20. Tsuboi, S., Komatitsch, D., Ji, C. & Tromp, J. Broadband modeling of the 2002 Denali, Alaska Mw 7.9 earthquake on the Earth Simulator. *Phys. Earth Planet. Inter.* **139,** 305–313 (2003).
21. Mazzotti, S. *et al.* Current tectonics of northern Cascadia from a decade of GPS measurements. *J. Geophys. Res.* **108,** 2554, doi:10.1029/2003JB002653 (2003).
22. Kao, H., Shan, S.-J., Rogers, G. & Dragert, H. Migration characteristics of seismic tremors in the northern Cascadia margin. *Geophys. Res. Lett.* **34,** L03304, doi:10.1029/2006GL028430 (2007).
23. Brodsky, E. E. & Prejean, S. G. New constraints on mechanisms of remotely triggered seismicity at Long Valley Caldera. *J. Geophys. Res.* **110,** B04302, doi:10.1029/2004JB003211 (2005).
24. Gomberg, J., Reasenberg, P. A., Bodin, P. & Harris, R. A. Earthquake triggering by seismic waves following the Landers and Hector Mine earthquakes. *Nature* **411,** 462–466 (2001).
25. Liu, Y. & Rice, J. R. Spontaneous and triggered aseismic deformation transients in a subduction fault model. *J. Geophys. Res.* (submitted).
26. Dragert, H., Wang, K. & Rogers, G. Geodetic and seismic signatures of episodic tremor and slip in the northern Cascadia subduction zone. *Earth Planets Space* **56,** 1143–1150 (2004).

Supplementary Information is linked to the online version of the paper at www.nature.com/nature.

Acknowledgements H. Kao, G. Rogers and H. Dragert provided comments and data that assisted with the tremor source location. Comments from W. McCausland, N. Beeler and H. Houston improved this manuscript. The data used in this study come from the Canadian National Seismograph Network and are distributed freely by The Geological Survey of Canada. This work was inspired by conversations with T. Pratt.

Author Contributions J.L.R. and J.E.V. found and identified the tremor, J.G. and P.B. computed the fault plane stresses, K.C.C. located the tremor source, and J.L.R. performed the spectral analysis. J.L.R., with the help of all, integrated the results.

Author Information Reprints and permissions information is available at www.nature.com/reprints. The authors declare no competing financial interests. Correspondence and requests for materials should be addressed to J.L.R. (justin@ess.washington.edu).

SUPPLEMENTARY INFORMATION

Figure S1

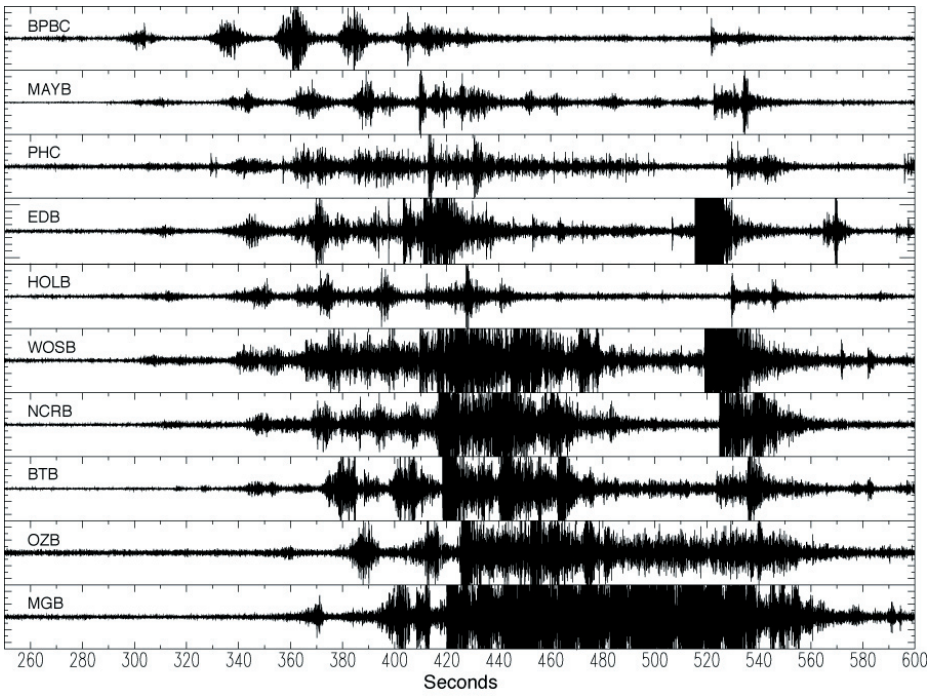

Figure S1: Record section showing moveout of triggered tremor — Section of 10 vertical seismograms arranged by distance from the triggered tremor, showing clear moveout of the tremor. Traces have been filtered between 5 and 15Hz and scaled to make the tremor easily identifiable. The additional impulsive bursts of energy at 420 and 520 s are triggered earthquakes in a different location than the tremor. Time is relative to 22:16 UTC.

Figure S2

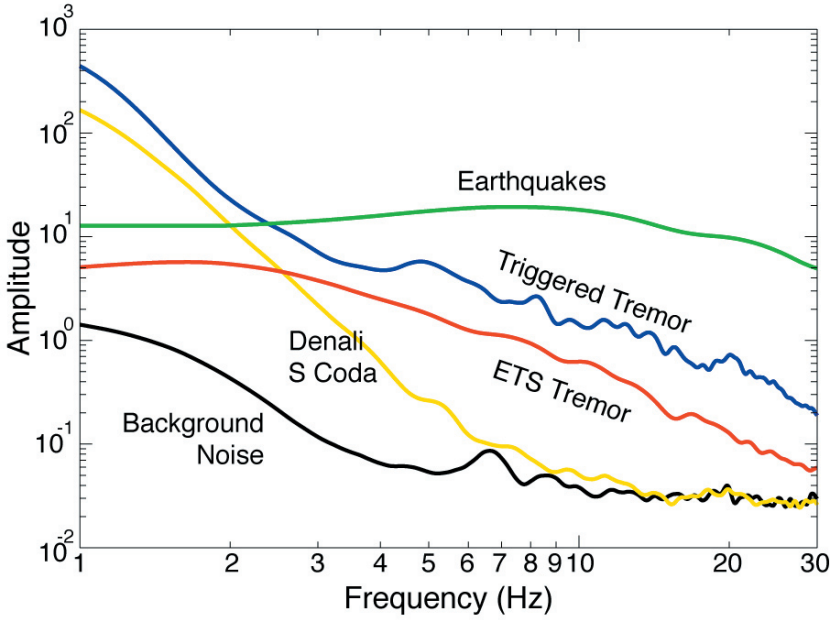

Figure S2: Comparison of Triggered Tremor/ETS Tremor/Earthquake/Noise Spectra — Comparison of linearly averaged, uncorrected spectra of vertical seismograms recorded at station MAYB of the *S* energy of 13 earthquakes, 5 typical ETS tremor episodes, the first four bursts of the triggered tremor, 4 windows of energy of the Denali *S* coda between the arrivals of the *S* and surface waves, and 2 windows just prior to the arrival of the *P* wave from Denali as background noise. The earthquakes we use are the 13 earthquakes within 10km of the epicenter of the triggered tremor that were recorded by MAYB between 11/1994 and 1/2007. These events range in magnitude from M_L 0.2 to M_L1.5. Assuming all of these events have a normal stress drop, the corner frequency for all of them should exceed 30Hz, so the slope that we are observing should be indicative of attenuation and not source processes. We use the 5 ETS tremor bursts in 2004-2005 that were within 30km of the epicenter for the triggered tremor (ETS tremor locations and timing provided by Kao *et al.,* 2007 and H. Kao, pers. comm.). Windows used to compute the spectra have varying length and their amplitudes have been normalized to a common window length of 2 seconds. Between 2Hz and 30Hz the triggered tremor and ETS tremor spectra are parallel, consistent with their arising from a common process. Below 2Hz the slope of the triggered tremor diverges from the ETS tremor due to the "noise" of the *S* coda and surface waves from the Denali Earthquake. Both kinds of tremor, though, are distinctly deficient in high frequencies relative to normal, high frequency earthquakes.

Figure S3

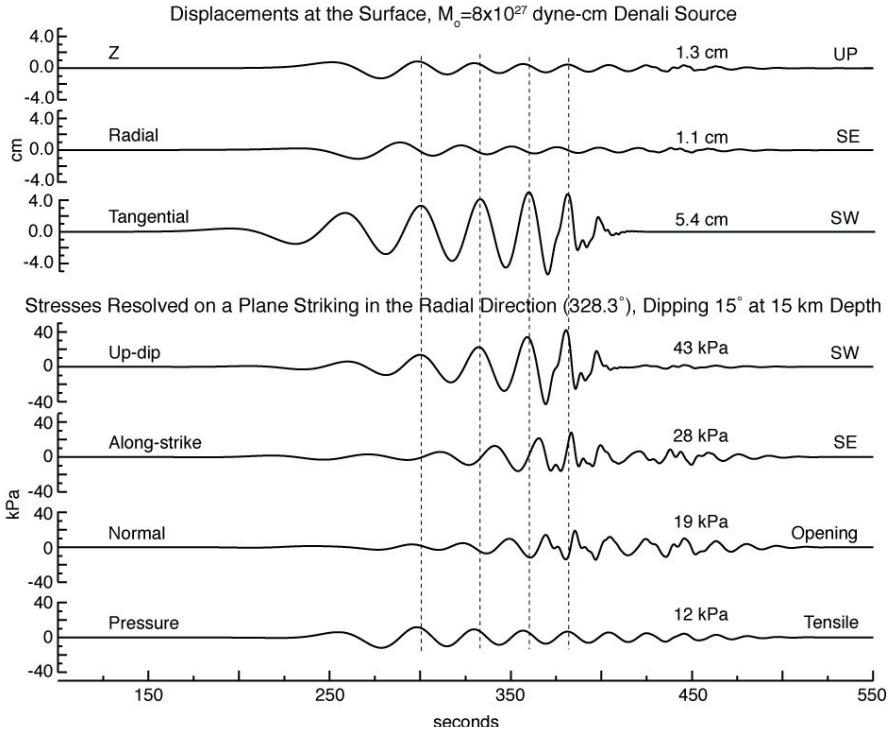

Figure S3: Synthetic displacements and stresses where the tremor is being generated — *Top panel*: Synthetic displacements at the surface. Estimated peak values of displacement are indicated for each component. *Bottom Panel:* Stresses at 15 km depth computed for a model of the Denali surface waves resolved onto the estimated megathrust plane. Maximum stresses are indicated for each component, with negative values indicating that the maximum stress is in the negative direction. Both panels: Time is relative to 22:16:00 UTC. Dashed, vertical lines indicate the peaks of the largest four pulses of the Love wave and the approximate timing of the centers of the four largest tremor bursts. Synthetics are computed using a locked-mode traveling wave algorithm for a point double-couple source at 7 km depth corresponding to a vertical, right-lateral, strike-slip fault striking at 114° (CW from N). Although the layered structure and source parameterization are much simpler than the true ones, the synthetics reproduce the important features of the wavefield near the region of interest; most significantly the Love waves are much larger than the Rayleigh waves before ~350 sec where the tremor is most prominent. The quality of the synthetic fit is examined in Supplemental Figure S4.

Figure S4

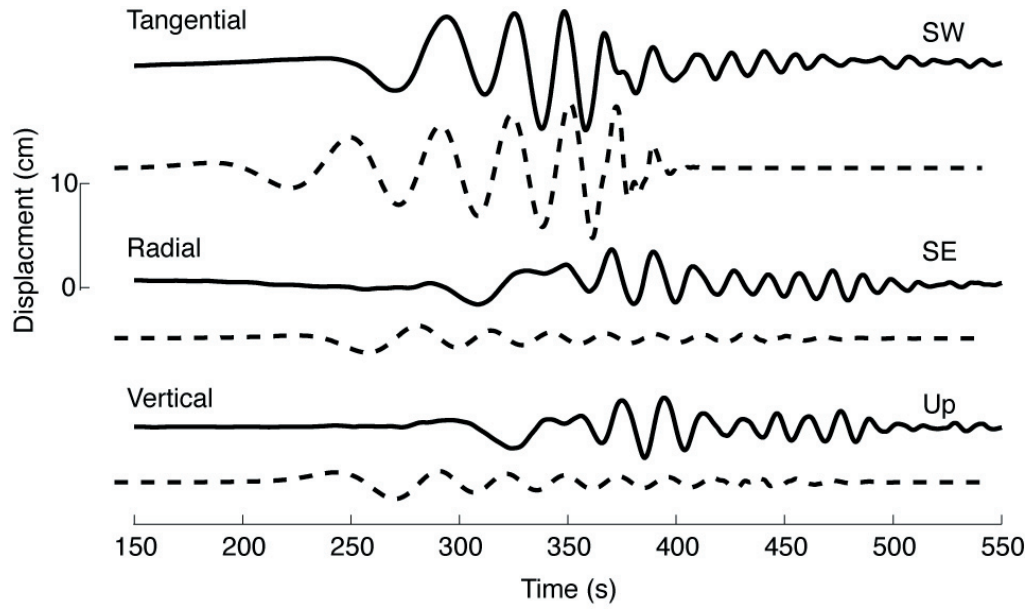

Figure S4: Synthetic vs. observed displacement at PHC — Comparison between displacement seismograms recorded at station PHC (solid) and calculated (dashed) for the same model as in the Supplementary Figure S3. The synthetics have been shifted so that they are in phase with the Love wave data (shift indicated by the offset in the start times), requiring a shift that can easily be attributed to source finiteness and inaccuracies in the modeled propagation along the ~1900 km path. Time is relative to 22:16:00 UTC. Note that the observed Rayleigh waves arrive much later than the synthetics, which indicates that their triggering of the tremor is even more unlikely than suggested by the synthetics.

Figure S5

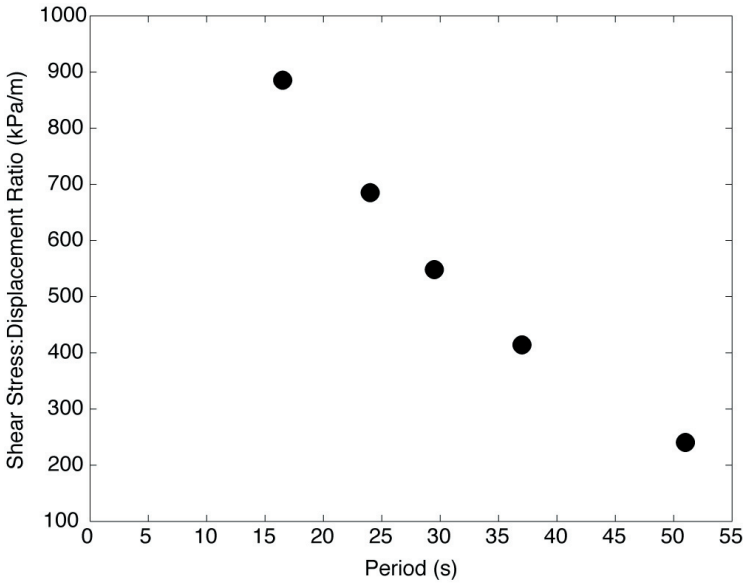

Figure S5: Ratio of maximum shear stress to maximum up-dip displacement for the five largest Love wave pulses — Using the synthetic seismograms from figure S3, we compute the ratio between up-dip shear stress resolved on the plate interface to displacement at the surface for the five largest Love wave pulses in the SW direction. Pulse period is determined using half-widths (from zero-crossings) of the displacement synthetic seismogram. Longer period (longer wavelength) waves stress the plate interface less than shorter period waves of equal amplitude. This arises because longer-wavelength Love waves penetrate more deeply than short period waves, making the displacement gradients—and hence stresses—at the relatively shallow plate interface smaller for long waves.